Iridium(III)porphyrin arrays with tuneable photophysical properties

M. Cidália R. Castro [a,*], Nabiha Ben Sedrine [b], Teresa Monteiro [b], Ana V. Machado [a]

[a] Institute of Polymers and Composites (IPC) and Institute of Nanostructures, Nanomodelling and Nanofabrication (i3N), University of Minho, Campus de Azurém, 4800-058 Guimarães, Portugal

[b] Physics Department and Institute of Nanostructures, Nanomodelling and Nanofabrication (i3N), University of Aveiro, Campus Universitário de Santiago, 3810-193 Aveiro, Portugal

Keywords:

Iridium porphyrin
Axial ligand effects
Optical sensor
NIR photoluminescence

Abstract

The photophysical properties of iridium(III) porphyrins complexes with two different axial ligands (Cl(CO) and bipyridine (bpy)) in solution and in cellulose acetate polymer matrix were investigated. The axial ligands substitution was made aiming to evaluate the photophysical properties and the solubility in different solvents. Therefore, dissimilar from the free porphyrin, non-polar solvents (as toluene) favours the quantum yield of iridium(III) porphyrins and ligands with a more extended π-conjugated compound as bpy results in higher yields. Moreover, despite all the porphyrins reveals a negative solvatochromism, the substitution of Cl(CO) ligand by by ligand exhibits similar solubility either on non-polar or polar solvents. The observed photoluminescence (PL) at room temperature appears at NIR region in contrast to the previously reported iridium(III) porphyrins. Comparing with free porphyrin H_2 TTP, the red/NIR PL spectra of the iridium(III)porphyrins (either in solution and in the polymer matrix) reveals remarkable changes. Particularly, a more significative decrease of the red/NIR intensity ratio was detected for $[Ir(ttp)(bpy)_2]2$ where the maxima of the NIR emission can be adjusted under suitable excitation wavelength.

Introduction

Luminescent materials based on iridium(III) complexes have become very attractive on design and development of new emitters for solid-state light applications. Iridium complexes not only arise as the most widely used class of emitters but also stand out from other complexes due to the advantage of their efficient and exclusively strong spin-orbit coupling parameter, high quantum yield and colourtuneable luminescence [1,2].

In the last years, porphyrins and related metalloporphyrins, a wellknown family essential in vital biological processes and with strong $\pi - \pi$ interaction that results in interesting photoluminescence properties, have increased attention both for biomedical and optoelectronic applications [3,4]. These macrocycles possess peculiar photochemical, photophysical, and photoredox properties: high radiative rate constants, large Stokes shift, visible absorption and emission bands, high luminescent quantum yields, low in vivo toxicity and their optical properties are tuneable through structural modifications [5]. Despite several studies have been made on nonplanar porphyrin complexes with more common metals ions, fewer have been addressed on porphyrins with d^6 metals ions, namely, on iridium complexes, mostly because synthesis and chemistry of these complexes are more difficult than the more commonly used metalloporphyrins. Actually, the combination of

Ir(III) as central metal and porphyrin is quite rare and only few groups have contributed to the synthesis, spectroscopic properties studies, and catalytic activities of these complexes [6-10]. Iridium(III) ion metal is hexacoordinated, which enables the possibility of introducing axial ligands directly on the metal. These can change the complex solubility or introduce new binding groups to improve the photophysical properties, efficiency and versatility. Therefore, through the appropriate choice of the ligand framework, it is possible, to control the emitting properties of the Ir(III) complexes [1,2,11].

The versatility of Ir(III) complexes allow to achieve three main objectives in optical sensing phase: i) tune the colour emission; ii) link covalently and/or non-covalently the iridium complex to solid supports in order to avoid aggregation and leaching of the dye; and iii) improve the compatibility among the complex and the solid support to decrease dye aggregation effects. Consequently, the advance on the Ir(III) chemistry, motivated by the improvement of new organic light emitters, has also enabled the development of Ir(III)-based materials for probes and sensing phases, where the immobilization of the Ir(III) complex into a solid material induces a higher mechanical stability and improves the material optical properties [1].

The first optical sensor material using an Ir (III) complex immobilized in polystyrene was reported by Vanderdonckt et al. in the 90's [2,12]. After that, Ir(III) complexes were immobilized in other polymeric matrix, such as poly(ethyleneglycol) ethyl ether methacrylate, poly (methyl methacrylate), poly(dimethylsiloxane), poly(1-trimethylsily-(lr(ttp)(bpy)2]

Scheme 1. Structures of H_2TTP, [Ir(ttp)Cl(CO)]1 and [Ir(ttp)$(bpy)_2$]2.

1-propyne)polyvinyl chloride, cellulose derivatives, etc. [13-17] Cellulose derivatives are popular for optical sensing applications due to its physical/mechanical properties and non-toxicity [18,19]. The selectivity, sensitivity and speed of bleaching of the sensor can also be regulated by choosing different matrices. This can either be achieved by covalent binding of the dye to the matrix or just by dispersion of a hydrophobic dye in a hydrophobic matrix.

Herein, we investigate the luminescence response of iridium(III) porphyrins, previously synthesized by our group, at room temperature under distinct excitation energies [20]. Moreover, the effect of two different ligands, (CO(Cl) and 4,4-bipyridine) and the immobilization on a cellulose acetate matrix on the iridium(III)porphyrins photophysical properties is also study.

Experimental

Materials and reagents

The cellulose acetate (Mn ~ 50,000) and meso-tetraphenylporphyrin was purchased from Sigma Aldrich. The solvents used: toluene (99.99%), acetone (99.99%), N,N-dimethylacetamide (DMAc) (99.88%), ethanol (99.80%), chloroform (99.99%) and N,N-dimethylformamide (DMF) (99.99%) were acquired from Fisher Chemical and used without further purification.

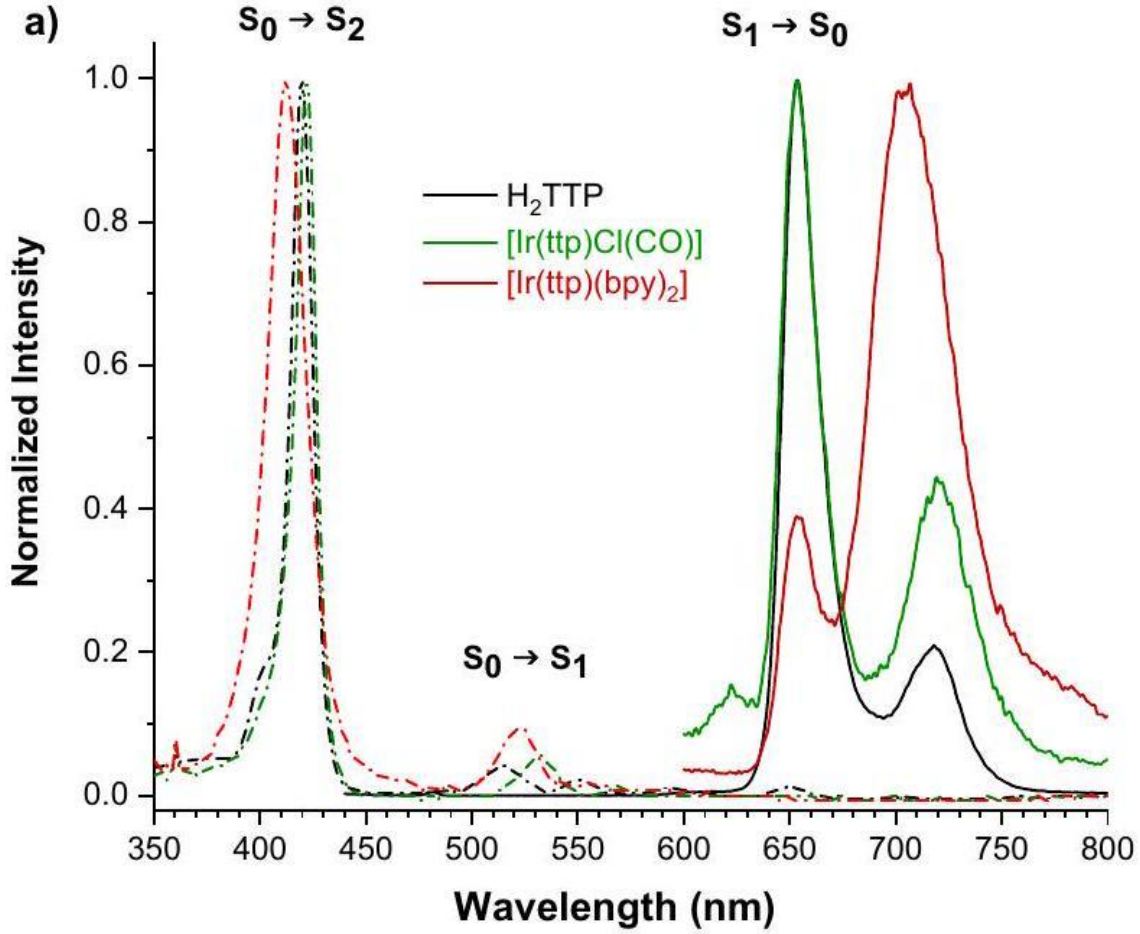

Preparation of the CA solutions and films

Synthesis and detailed characterization of chloro(5,10,15,20tetratolylporphyrinato)carbonyliridium(III) [Ir(ttp)Cl(CO)]1 and (5,10,15,20-(tetratolylporphyrinato)(bipyridine) $_2$ iridium(III) [Ir(ttp) $(bpy)_2$]2 was already reported by our group (Scheme 1) [20]. Here it was possible to demonstrate, either through mass (MALDI-TOF MS) and ^{1}H NMR spectroscopy techniques, the coordination of iridium ion on the porphyrin core with Cl(CO) as axial ligand and the consequent substitution with two bipyridine yielding [Ir(ttp)Cl(CO)]**1** and [Ir(ttp) $(bpy)_2$]2, respectively.

The CA solutions were prepared using a mixed-solvent system, acetone/dimethylacetamide (DMAc) in a ratio of 2/1, at room temperature (RT) with constant concentration of CA of 12wt%. From solutions prepared with CA and porphyrins, 5wt% of H_2TTP, [Ir(ttp)Cl(CO)]**1** and [Ir(ttp)$(bpy)_2$]2 were added relative to CA weight. Homogeneous solutions were obtained after at least 12 h of stirring. Part of all the solutions were transferred into a Petri dish and kept at room temperature during 4 days for solvent evaporation. Coloured transparent and detachable thin films (24μ m) were obtained.

Measurements and instrumentation

Absorption spectra, in the wavelength range of $250 - 700$ nm, were measured using a Shimadzu UV-2401PC UV-Visible spectrophotometer

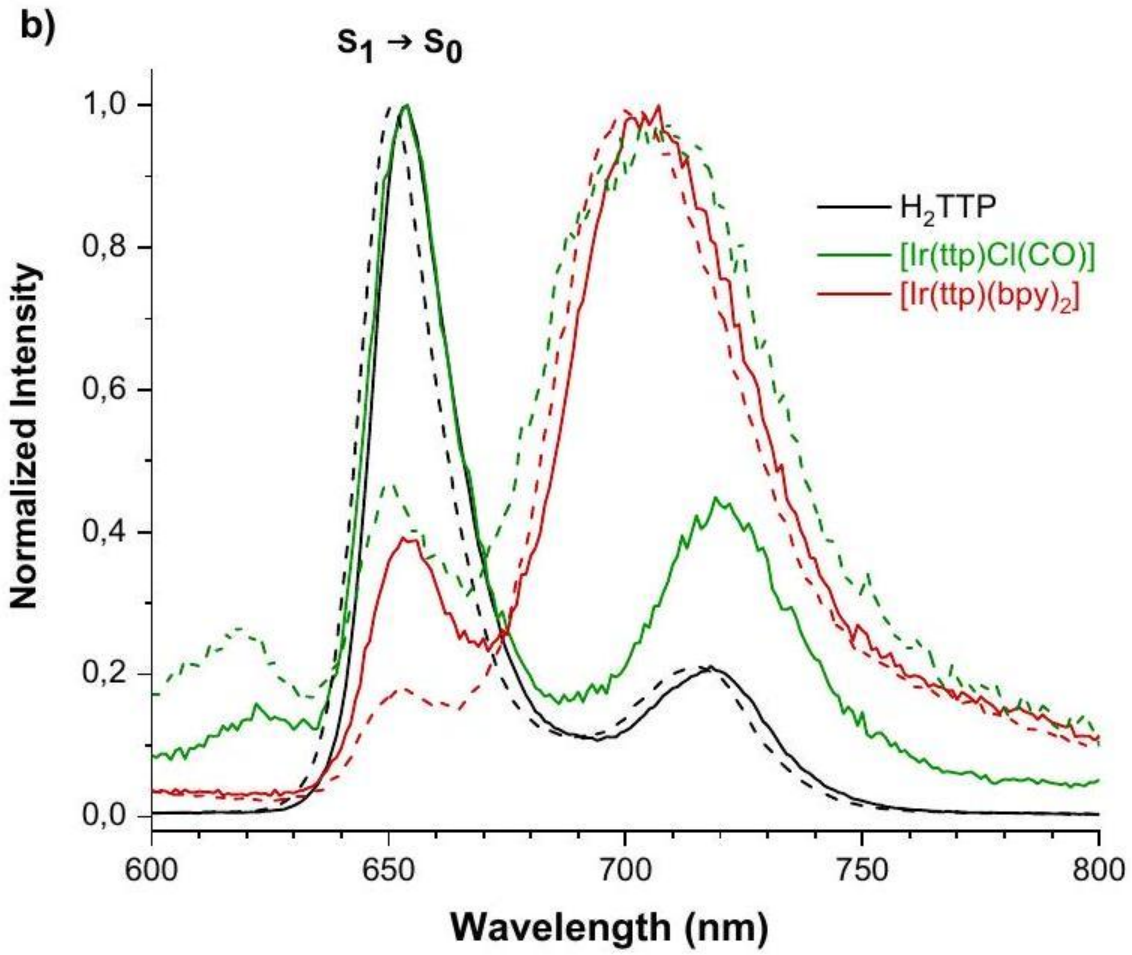

Fig. 1. a) Normalized absorption (dashed lines) and PL spectra (solid lines) of H_2TTP (black), [Ir(ttp)Cl(CO)]**1** (green) and [Ir(ttp)(bpy)$_2$]**2** (red) solutions in toluene. b) Comparison of the normalized PL spectra of H_2TTP (black), [Ir(ttp)Cl(CO)] **1** (green) and [Ir(ttp)(bpy) $_2$] **2** (red) solutions in toluene (solid lines) and in ethanol (dashed lines). The PL spectra were obtained upon excitation in the band maxima of the Soret absorption band.

using toluene, ethanol, chloroform and DMF as solvents. Steady state photoluminescence (PL) was measured using two different systems: a FluoroMax-4 and a Fluorolog-3 from Horiba Scientific. The former was also used to quantity PL quantum yields. The excitation beam was directed into a thin cell with a 10 mm excitation path length and was focused slightly with a quartz lens to a point close to the front wall of the cell, from which emission was analysed. To minimize reabsorption of $S_{1,2} - S_0$ emission, the beam diameter at focus was between 2 and 5 nm for solutions and 10 nm for films. Under these conditions, measurable reabsorption of emission could be detected using concentrations from 2×10^{-7}M to 1×10^{-6}M. The quantum yield, Φ, is defined as the ratio of number emitted photon by the absorbed ones, that corresponds to the ratio of the radiative transition probability to the total one, $\Phi = k_r/(k_r + k_{nr})$, where the k_r and k_{nr} stands for the radiative and nonradiative transition rates. Fluorescence quantum yields were measured using a comparative method considering a reference standard with emission and absorbance properties similar to the ones to be tested in the porphyrin compounds. For such purpose the integrated fluorescence intensities of the porphyrin complexes (I_F) and reference standard (I_R) were used as well as their absorbance values (A_F, A_R) and the

reference standard quantum yield (Q_R) were used according to $\Phi_F = \Phi_R[(I_F A_R)/(I_R A_F)]$. A solution of tetraphenylporphyrin in toluene (1×10^{-4}M) as used as standard ($\Phi_R = 0.13$ [21]) and corrected to the refraction index of the solvents. For the quantum yields determination, the fluorescence standard was excited at the wavelengths of maximum absorption found for each one of the compounds to be tested and in all fluorimetric measurements the absorbance of the solution did not exceed 0.1. The Fluorolog-3 system was used to analyse PL and PL excitation (PLE) spectra. The apparatus has a double additive grating Gemini 180 monochromator (1200 grooves. mm^{-1} and 2×180 mm) in the excitation and a triple grating iHR550 spectrometer in the emission (1200 grooves. mm^{-1} and 550 mm). A 450 W Xe arc lamp was used as excitation source. PLE was assessed by varying the excitation energy and monitoring the energy at the maxima of the PL emission bands. Time resolved PL (TRPL) were acquired with the same Fluorolog-3 system using a pulsed Xe lamp coupled to a monochromator. All the spectra were taken at RT and were corrected for the spectral response of the optical components and the Xe lamp.

Results and discussion

Uv-vis and PL properties of synthesized Ir(III)porphyrins

The photophysical properties of Ir (III) porphyrins differ significantly from others cyclometalated Ir(III) compounds and other group 9 metal porphyrin complexes, which is due to the closed shell diamagnetic d^6 configuration [10]. The literature reports that d^6 metalloporphyrins exhibits red to near-infrared luminescence (NIR) derived from the $^3(\pi,\pi^*)$ intraligand state of the porphyrin ligand or the $^3(d\pi,\pi^*)$ metal-to-ligand charge transfer (MLCT) state upon photoexcitation [22]. In the case of Ir (III)porphyrin complex derivatives, previously reported works reveal that the complexes exhibit a strong red to NIR PL in solution at room temperature, with an emission quantum yield up to 0.85 [9,10,23,24]. The optical properties of organic compounds are set through their energy gap, i.e., the energy separation among the highest occupied molecular orbital (HOMO) and lowest unoccupied molecular orbital (LUMO) (HOMO-LUMO energy gap). The keystone for designing potential NIR emitters is based on reducing the energy gap, resulting in a red shift of absorption and emission spectra. Therefore, for NIR fluorescent molecules in general, some features should be taken into attention, such as the π-conjugation length, bond length alternation, conformation, and the presence of donor-acceptor system [25].

Figs. 1 and 2 show the absorption spectra of the free porphyrin H_2 TTP, [Ir(ttp)Cl(CO)]**1** and [Ir(ttp)$(bpy)_2$]**2** solutions in different solvents. As it can be seen, the spectra are dominated by the porphyrin based visible Q (ca. 480-650 nm) and Soret (ca. 380-450 nm)

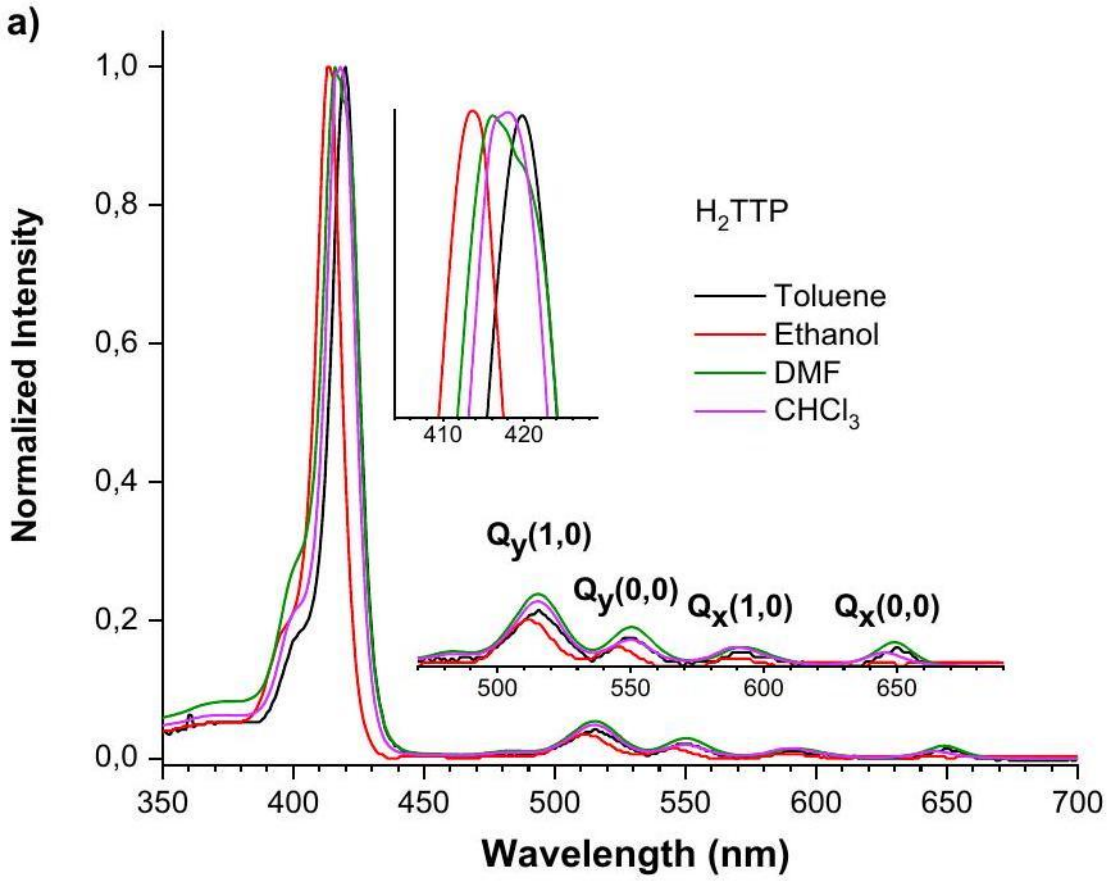
a)
Normalized Intensity
1,0
0,8
0,6
0,4
0,2
0,0
350
400
450
500
550
600
650
700
Wavelength (nm)
H2TTP
Toluene
Ethanol
DMF
CHCl3
410
420
Qy(1,0)
Qy(0,0)
Qx(1,0)
Qx(0,0)
500
550
600
650

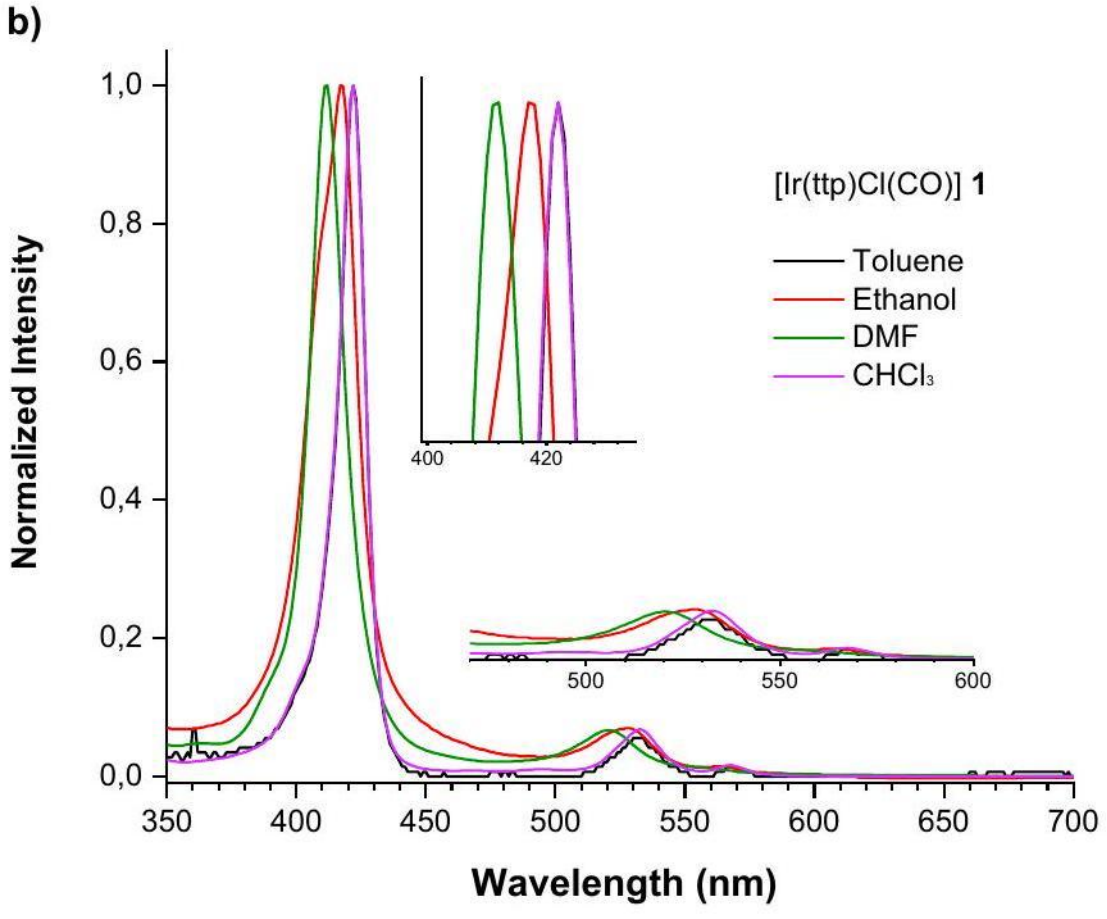
b)
Normalized Intensity
1,0
0,8
0,6
0,4
0,2
0,0
350
400
450
500
550
600
650
700
Wavelength (nm)
[Ir(ttp)Cl(CO)] 1
Toluene
Ethanol
DMF
CHCl3
400
420
500
550
600

Fig. 2. UV-visible normalized absorption spectra of a) H_2TTP, b) [Ir(ttp)Cl(CO)]**1** and c) [Ir (ttp)$(bpy)_2$]2 in four solvents of different polarity (toluene, ethanol, chloroform and DMF).

Table 1
Solvatochromic data [λ_{max} (nm) and Δv_{max} (cm^{-1}) of the Soret band] for H_2TTP, [Ir(ttp)Cl(CO)]**1** and [Ir(ttp)$(bpy)_2$]**2** in four solvents with π^* values by Kamlet and Taft [32].

Compound	Toluene (0.535)		Ethanol (0.540)		Chloroform (0.760)		DMF (0.875)		Δv_{max} [a]
	λ_{max} [r	v_{max} [cr	λ_{max} [r	v_{max} [cr	$\lambda_{máx}$ [r	v_{max} [cr	λ_{max} [r	v_{max} [cr	
H_2 TTP	420	23,810	415	24,096	419	23,866	416	24,038	-229
1	422	23,697	417	23,981	422	23,697	412	24,272	-575
2	412	24,272	408	24,510	412	24,272	411	24,331	-59

[a] $\Delta v_{max} = v_{max}$ (Toluene) $- v_{max}$ (DMF)/cm^{-1}.

absorption bands due to $\pi \rightarrow \pi$ *electronic transitions from the ground to the first and second excited states, $S_0 \rightarrow S_{1,2}$, respectively [26,27]. Five Q absorption transitions can be detected for the free porphyrin H_2TTP in toluene (Figs. 1a) and 2a)), peaked at 648 nm, 592 nm, 548 nm, 514 nm, 482 nm. These zero phonon (0,0) and vibronic overtones (n, 0) transitions are assigned to $Q_x(0,0), Q_x(1,0), Q_y(0,0), Q_y$ (1,0) and $Q_y(2,0)$ respectively, due to the splitting of the free porphyrin electronic states under low molecular symmetry (D_{2h})[27,28]. Additionally, the most intense absorption band maximum is peaked at 420 nm (with a small shoulder ca. 400 nm), and corresponds to the Soret or B band. In the case of metalloporphyrins d [6], as Ir(III) porphyrins, these absorption bands are known to usually display noticeable hypsochromic shifts, with respect to the absorption peak position of their free base porphyrins, due to dπ (metal) $-\pi^*$ (porphyrin) interaction [22,29]. However, the number of observed Q absorption bands in metalloporphyrins is known to be strongly dependent on the coordination symmetry. Therefore, a decrease of the absorption transitions number upon insertion of the metal ion inside the macrocycles is usually perceived, due to the degeneracy of the electronic states under a higher symmetry coordination (D_{4h}) [27]. Moreover, previous work from our group [20] and other authors [7,8,22,30], demonstrate that axial ligands modulate the electronic properties of the metal ion and consequently the metal-porphyrin bonding interaction, resulting in noticed changes of the absorption spectra. Indeed, from Fig. 1a), it is possible to see that, besides the reduced number of Q absorption bands upon metalation, the peak position of the absorption bands of Ir(III) porphyrins complexes exhibit blue or red shift when compared with the one of the H_2 TTP. Particularly, a red shift of the Soret and Q bands occurs with Cl(CO) ligands (Soret: 422 nm ; Q bands: 531 nm, 567 nm), while a noticed blue shift of the Soret band and a red shift of the Q band is observed with bpy ligand (Soret: 412 nm ; Q bands: 522 nm, 557 nm). This behaviour is

in good agreement with the reported tendency for changes

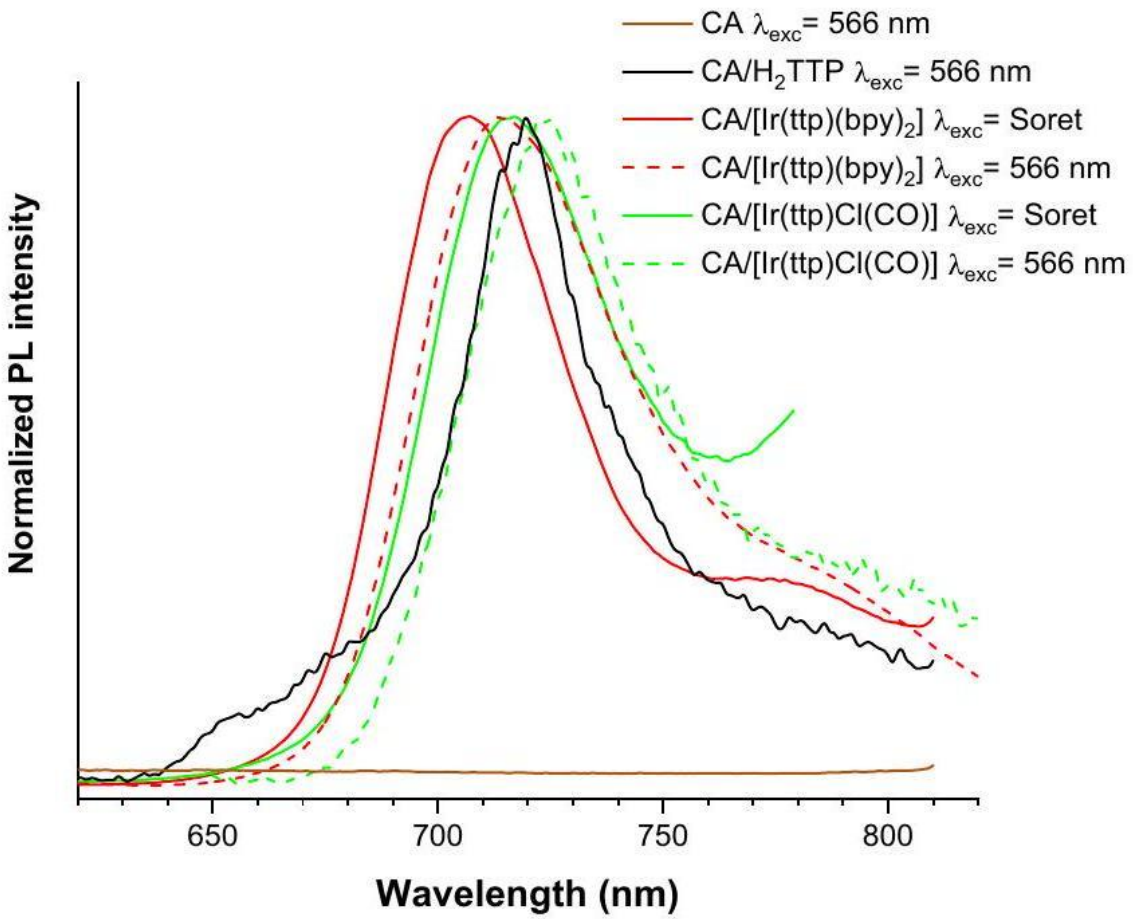

Fig. 3. PL spectra of CA, CA/ H_2TTP, CA/[Ir(ttp)Cl(CO)] and CA/[Ir(ttp)(bpy)$_2$] films obtained with excitation at the Soret absorption band maxima (ca. 420 nm) and Q band (ca. 566 nm).

in the environment polarity, namely while electron-withdrawing groups tend to stabilize the HOMO through electron density removal from the metal inducing a blue shift of absorption, donating groups have the opposite effect [20].

Furthermore, Fig. 1a) and b) display the PL spectra of porphyrins in toluene and ethanol solvents. Upon excitation at the porphyrin Soret absorption band maximum, the H_2TTP and [Ir(ttp)Cl(CO)]**1** in toluene exhibit two main emission bands at lower energies, in the red and NIR spectral regions, evidencing that a fast internal conversion from S_2 to S_1 electronic states occurs. PL maxima in the red (Q(0,0) at 654 nm) and NIR (Q(0,1) at 720 nm) spectral regions due to the $S_1 \rightarrow S_0$ transitions from the porphyrin's were identified [22,27]. For H_2 TTP, a Stokes shift of ca. 142 cm^{-1} was estimated from the difference between the $S_0 \leftrightarrow S_1$ absorption and emission spectra. Despite the changes in the absorption spectra due to increased coordination symmetry of the metalloporphyrin, the PL spectrum of the [Ir(ttp)Cl(CO)]1 complex shows a spectral shape and full width at half maxima (FWHM) of ca. 60 meV similar to the one of the H_2 TTP suggesting alike recombination process. [Ir(ttp)Cl(CO)]**1** also exhibits a minor intensity PL emission at shorter wavelengths peaked ca. 620 nm . For [Ir(ttp)(bpy)$_2$]2 in toluene the red and NIR

PL maxima occur at 654 nmQ(0,0) and 706 nm with a tail extending to longer wavelengths. While the high energy electronic transition has a FWHM similar to the ones observed in H_2 TTP and [Ir (ttp)Cl(CO)] 1, the FWHM of the band at lower energies (ca. 110 meV) suggests that the NIR recombination may arise from a distinct process, involving electronic states that lie at lower energies than the S_1, as is typically the case of triplets responsible for Iridium-based phosphorescence. It should be emphasized that, for the same solvent, and replacing the porphyrin ligand Cl(CO) for bpy, the PL spectra reveal a noticed decrease of the red (654 nm) emission intensity. Nevertheless, and as shown in Fig. 1b), changing the solvent from aprotic (toluene) to protic (ethanol), the PL spectral shape for the H_2 TTP remains the same only with a slight blue shift. Conversely, the spectra of the [Ir(ttp)Cl(CO)]**1** and [Ir(ttp)$(bpy)_2$]2 complexes exhibit the same tendency under Soret excitation: i) quenching of the red 654 nm emission band and ii) increase of the FWHM of the NIR emission peaked ca. 706 nm . An additional 620 nm emission band is detected for Cl(CO) porphyrin ligand. Therefore, both axial ligands and nature of the solvents used play an important role in the modification of the red/NIR PL properties of the studied porphyrins. The decrease of the red/NIR intensity ratio was found to be more pronounced in the case of the bpy than in Cl(CO) ligand. This is in agreement with previously reported works, once the introduction of polar and more conjugated groups as axial ligands results in wellsoluble compounds in organic solvents and consequently in differences on photophysical and photochemical properties [7,8,10,31].

The PL quantum yields at room temperature for H_2TTP, [Ir(ttp)Cl(CO)] 1 and [Ir(ttp)$(bpy)_2$]2 for Soret band both in toluene and ethanol were calculated and compared with the standard used, tetraphenylporphyrin ($\Phi_F = 0.13$ in toluene solution at RT) [21]. The PL quantum yield for H_2 TTP in toluene is similar to the standard used ($\varphi_F = 0.15$), however, it increases up to $\Phi_F = 0.17$ when ethanol is used as solvent. The coordination with iridium ion on porphyrin core, the consequent ligand exchange and the nature of solvent used results in a different performance of the PL quantum yield. Toluene enhances the quantum yields of the complexes [Ir(ttp)Cl(CO)]**1** and [Ir(ttp)(bpy)$_2$]**2** for $\Phi_F = 0.0012$ and $\Phi_F = 0.0036$, respectively. Whereas, in ethanol solutions, the quantum

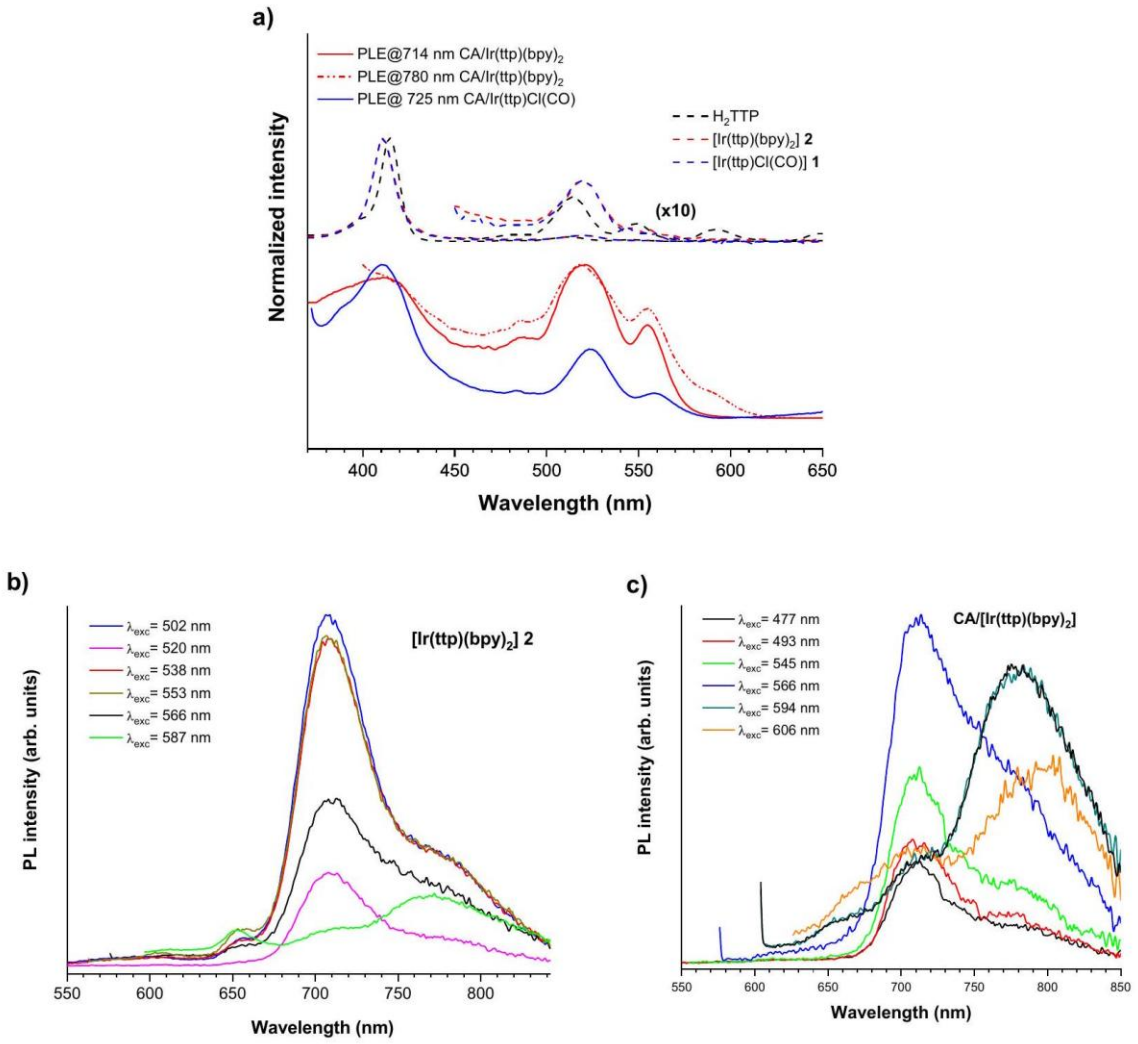

Fig. 4. a) PLE spectra monitored at the NIR emission bands of the CA/[Ir(ttp)(bpy) $_2$] and CA/[Ir(ttp)Cl(CO)] films; for comparison the absorption spectra of the H_2TTP and Ir(II) porphyrin complexes in solution was included. b, c) Wavelength excitation dependent PL spectra for [Ir(ttp)$(bpy)_2$]2 and CA/[Ir(ttp)(bpy)2], respectively. yields decrease to $\Phi_F = 0.00072$ for [Ir(ttp)Cl(CO)]**1** and $\Phi_F = 0.0026$ for [Ir(ttp)$(bpy)_2$]2. Comparing the two types of ligands used, the substitution for an extended π-conjugated bpy ligand at the axial positions, results in a significant increase on the PL quantum yield.

Analysis of the polarity effect on Ir(III)porphyrins

A study of the porphyrins absorption in four solvents with different polarities was realized to investigate the polarity effect of H_2TTP, [Ir(ttp) Cl(CO)]**1** and [Ir(ttp)$(bpy)_2$]**2** in solution, as shown in Fig. 2. The absorption wavelength maxima λ_{max} of these compounds are summarized in Table 1 and were compared with the π^* values for each solvent, as determined by Kamlet and Taft [32]. All the studied compounds exhibit negative solvatochromism ($\Delta\nu_{max}$ from -575 to -59 cm^{-1}), which corresponds to a hypsochromic shift with increasing solvent polarity. From the results, it is possible to observe that the most significant change of the porphyrin's behaviour in different solvents is obtained for [Ir(ttp)Cl(CO)]**1** compound, with $\Delta\nu_{max} = -575$ cm^{-1}, whereas [Ir(ttp)$(bpy)_2$]2 reveals a

similar behaviour either in nonpolar or polar solvents. This behaviour evidences that the energy of the electronic states is sensitive to the external substituent and is due to a higher stabilization of the excited state relatively to the ground state.

PL and PLE properties of porphyrins in CA films

The as-synthesized porphyrins were further immobilized in CA films. Fig. 3 shows the PL spectra of CA, CA/ H_2TTP, CA/[Ir(ttp)Cl(CO)] and CA/[Ir(ttp)$(bpy)_2$]. Embedding the free porphyrin H_2 TTP in CA results in a perceived decrease of the red (654 nm)/NIR (720 nm) emission when the 566 nm excitation (Q band) is used. For CA/Ir(III) porphyrin complexes, the peak position of the emission bands was found to be dependent on the excitation wavelength. By exciting the samples at the maxima of the Soret band, the peak position of the broader NIR emission occurs at the same value as the ones detected in toluene (Fig. 1). However, a noticed red shift is observed by changing the wavelength excitation to lower energies, namely by exciting the samples at the Q band maxima. Moreover, the shoulder observed at longer wavelengths is more pronounced. For comparison purposes, the spectrum of the CA obtained under the same $+Q$ excitation conditions is also shown, revealing, as expected, that these standard film does not show emission in this spectral region.

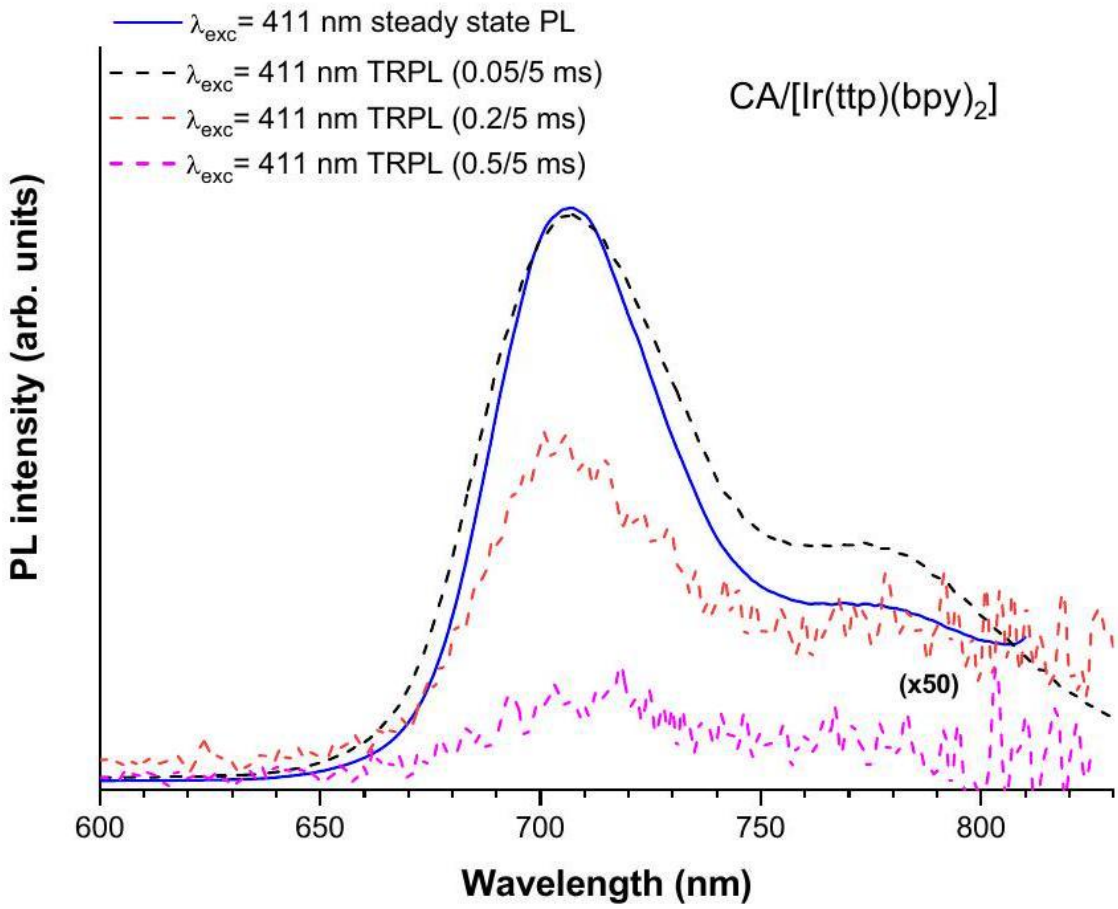

Fig. 5. Comparison between the steady state PL and TRPL spectra of the CA/[Ir(ttp)(bpy)$_2$] film obtained upon excitation on the Sorbet band. TRPL spectra were measured

considering a time window of 5 ms with increasing delay times from 50μ s to 500μ s. Similar spectra (not shown here) were obtained using green 520 nm excitation.

To gain insights into the population paths of the NIR luminescence for the [Ir(ttp)$(bpy)_2$]2 and [Ir(ttp)Cl(CO)]**1** metalloporphyrins after immobilization in CA, PLE spectra were monitored at the emission maxima in solid samples, as depicted in Fig. 4a). The results clearly evidence that after immobilization and besides the enlarged Soret band, the NIR luminescence is preferentially populated through the green/orange and red excitation bands. The spectra exhibited in Fig. 4b, c) illustrate the wavelength excitation-dependent PL spectra for the samples with highest PL intensity, [Ir(ttp)$(bpy)_2$]2, either in solution (on the same mixture of solvent used to prepare the CA films (acetone/DMAc 2/1)) and immobilized in CA films, respectively. As aforementioned, the peak position of the long wavelength recombination can be tuned by an appropriate choice of the excitation wavelength, suggesting that the broad PL bands arise from different emitting states than the singlet ones.

This hypothesis was verified using TRPL for the solid film CA/[Ir(ttp) $(bpy)_2$], as presented in Fig. 5. By exciting the sample at the Soret band with a pulsed Xe lamp for a time window of 5 ms , it can be seen that, the NIR luminescence bands peaked ca. 706 nm and 780 nm can still be observed after a delay of 50μ s. Furthermore, the fact that the 1/e emission
intensity strongly quenches for delays higher than 200μ s means that the recombinations at longer wavelengths are slow (with lifetimes of tens to hundreds of μs) and may arise from spin forbidden recombination's (e.g. a mixed [3]MLCT/ [3]LLCT to the ground state), which is not the case of the fast singlet-singlet transitions. Therefore, in the samples studied here the triplet recombination process appears to be responsible for the broad PL bands in the NIR spectral region.

For the case of the Cl(CO) ligand, the PL intensity in solution is lower than the one of the porphyrin coordinated to bpy but even so, the NIR luminescence bands dominate the PL spectra when the [Ir(ttp)Cl(CO)] is immobilized in CA, as indicated in Fig. 6.

Conclusions

Spectroscopic and photophysical properties of H_2 TTP and iridium (III) complexes with two different ligands Cl(CO) and 4,4-bipyridine were investigated. Compared with the H_2TTP, the Q and Soret absorption bands in Ir(III) porphyrins evidence blue and red shifts. Moreover, the results of the study of polarity effect demonstrate that all the porphyrins reveal a negative solvatochromism, consistent to a hypsochromic shift with increasing solvent polarity. The quantum yield of Ir(III) porphyrins both in toluene and ethanol increase with the introduction of extended π-conjugated ligands as bpy.

When compared with the H_2 TTP, the red/NIR PL spectra of the Ir(III) porphyrins were found to undergo noticed changes. Mainly, the increase of the full width at half maximum of the NIR emitting bands reveals that the longer wavelength recombination involves additional emitting states when compared with the typical $S_1 \rightarrow S_0$ transition of the H_2 TTP. The decrease of the red/NIR intensity ratio was found to be more pronounced in the case of the bpy ligand and wavelengthdependent excitation measurements evidence that the maxima of the NIR recombination can be tuned under appropriate excitation. The same behaviour was detected in the porphyrins immobilized dispersed in cellulose acetate,

evidencing the two main emitting broad bands peaked at ca. 706 nm and 780 nm . Time resolved spectroscopy demonstrate that these two recombination processes are slow, with lifetimes of the order of hundreds of microseconds, suggesting that the emission arises from spin forbidden recombination's, e.g. a mixed [3]MLCT/ [3] LLCT to the ground state.

These results demonstrated the versatility of these complexes to tunable their photophysical properties for application as a biocompatible and biodegradable oxygen probe. These complexes are promising as indicators for oxygen sensors with tailor-made sensitivity.

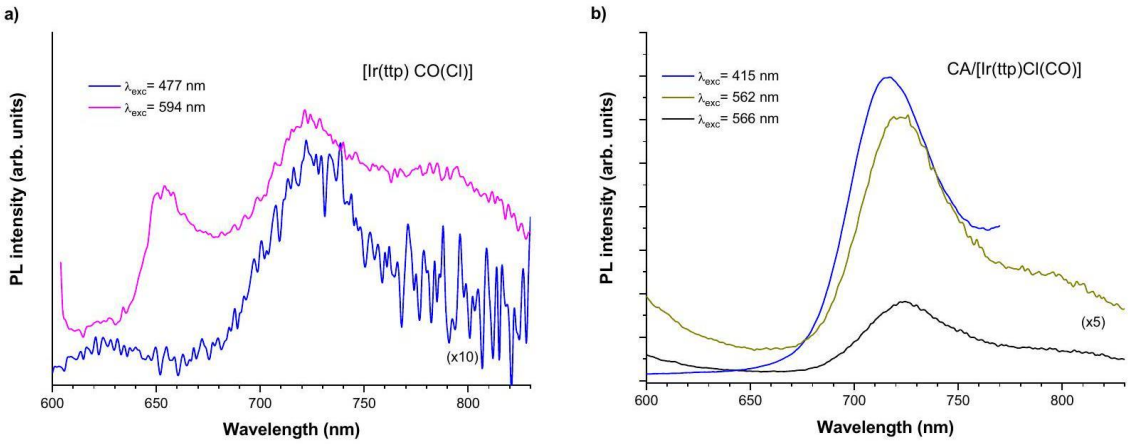

Fig. 6. Wavelength dependent PL spectra of a) [Ir(ttp)CO(Cl)]1 in solution and b) CA/Ir(ttp)CO(Cl) solid film.

Acknowledgements

This work was developed within the scope of the project TSSiPRO technologies for sustainable and smart innovative products - NORTE-01-0145-FEDER-000015 and the project i3N, UIDB/50025/2020 & UIDP/50025/2020, financed by national funds through the FCT/MEC.

References

[1] S. Teets, T., in: Eli Zysman-Colman (Ed.), Iridium(III) in Optoelectronic and Photonics Applications. 2 Volume Set, 2, , 2018.
[2] Z. Liu, Z. Bian, C. Huang, Luminescent Iridium Complexes and Their Applications, 28, 2009 113-142.
[3] M. Imran, M. Ramzan, A.K. Qureshi, M.A. Khan, M. Tariq, Emerging applications of porphyrins and metalloporphyrins in biomedicine and diagnostic magnetic resonance imaging, Biosensors 8 (4) (2018) 95.
[4] M. Danquah, Review of handbook of porphyrin science with application to chemistry, physics, materials science, engineering, biology and medicine. Volume 40: nanoorganization of porphyrinoids, J. Nat. Prod. 80 (4) (2017) 1232.
[5] W. Burda, L. Shaw, M. Shepherd, Porphyrins: properties and applications, Handbook of Chemistry, Biochemistry and Biology: New Frontiers, Nova Publishers 2012, pp. 429-

438.
[6] B.J. Anding, A. Ellern, L.K. Woo, Comparative study of rhodium and iridium porphyrin diaminocarbene and N-heterocyclic carbene complexes, Organometallics 33 (9) (2014) 2219-2229.
[7] T.-L. Lam, K.-C. Tong, C. Yang, W.-L. Kwong, X. Guan, M.-D. Li, V. Kar-Yan Lo, S. LaiFung Chan, D. Lee Phillips, C.-N. Lok, C.-M. Che, Luminescent ruffled iridium(iii) porphyrin complexes containing N-heterocyclic carbene ligands: structures, spectroscopies and potent antitumor activities under dark and light irradiation conditions, RSC 10 (1) (2019) 293-309.
[8] K. Koren, S.M. Borisov, R. Saf, I. Klimant, Strongly phosphorescent iridium(III)-porphyrins - new oxygen indicators with tuneable photophysical properties and functionalities, Eur. J. Inorg. Chem. 2011 (10) (2011) 1531-1534.
[9] J. Zhou, L. Gai, Z. Zhou, J. Mack, K. Xu, J. Zhao, H. Qiu, K.S. Chan, Z. Shen, Highly efficient near IR photosensitizers based-on Ir-C bonded porphyrin-aza-BODIPY conjugates, RSC Adv. 6 (76) (2016) 72115-72120.
[10] B.-B. Wang, H. Zuo, J. Mack, P. Majumdar, T. Nyokong, K.S. Chan, Z. Shen, Optical properties and electronic structures of axially-ligated group 9 porphyrins, J. Porphyrins Phthalocyanines 19 (8) (2015) 973-982.
[11] Adam F. Henwood, Z.-C. E., Photoluminescent materials and electroluminescent devices, in: N. Armaroli, H. Bolink (Eds.), Luminescent Iridium Complexes Used in Light-Emitting Electrochemical Cells, Springer International, 2018.
[12] E. Vanderdonckt, B. Camerman, F. Hendrick, R. Heme, R. Vandeloise, Polystyrene immobilized Ir(III) complex as a new material for optical oxygen sensing, Bull. Soc. Chim. Belg. 103 (5-6) (1994) 207-211.
[13] G. Di Marco, M. Lanza, M. Pieruccini, S. Campagna, A luminescent iridium(III) cyclometallated complex immobilized in a polymeric matrix as a solid-state oxygen sensor, Adv. Mater. 8 (7) (1996) 576-580.
[14] M.C. DeRosa, P.J. Mosher, G.P.A. Yap, K.S. Focsaneanu, R.J. Crutchley, C.E.B. Evans, Synthesis, characterization, and evaluation of [Ir(ppy)2(vpy)Cl] as a polymerbound oxygen sensor, Inorg. Chem. 42 (16) (2003) 4864-4872.
[15] H. Na, P.N. Lai, L.M. Cañada, T.S. Teets, Photoluminescence of cyclometalated iridium complexes in poly(methyl methacrylate) films, Organometallics 37 (19) (2018) 3269-3277.
[16] H. Na, Louise M. Cañada, Z. Wen, J. I-Chia Wu, T.S. Teets, Mixed-carbene cyclometalated iridium complexes with saturated blue luminescence, Chem. Sci. 10 (25) (2019) 6254-6260.
[17] Takeuchi, Y.; Amao, Y., Materials for luminescent pressure-sensitive paint. In Frontiers in Chemical Sensors Rontiers in Chemical Sensors. Springer Series on Chemical Sensors and Biosensors (Methods and Applications), Orellana G., M.-B. M. C., Ed. Springer: Berlin, Heidelberg, 2005; vol. 3, pp 303-322.
[18] X. Qiu, S. Hu, "Smart" materials based on cellulose: a review of the preparations, properties, and applications, Materials 6 (3) (2013) 738.
[19] S. Ummartyotin, H. Manuspiya, A critical review on cellulose: from fundamental to an approach on sensor technology, Renew. Sust. Energ. Rev. 41 (2015) 402-412.
[20] M.C.R. Castro, A. de Sá, A.M. Fonseca, M.M.M. Raposo, A.V. Machado, Development of iridium porphyrin arrays by axial coordination through N-bidentate ligand: synthesis and evaluation of the optical, electrochemical and thermal properties, Polyhedron 154 (2018) 302-308.
[21] D.J. Quimby, F.R. Longo, Luminescence studies on several tetraarylporphins and their zinc derivatives, J. Am. Chem. Soc. 97 (18) (1975) 5111-5117.
[22] L.M.A. Levine, D. Holten, Axial-ligand control of the photophysical behavior of

ruthenium(II) tetraphenyl- and octaethylporphyrin: contrasting properties of metalloporphyrin (.pi.,.pi.*) and (d,.pi.*) excited states, J. Phys. Chem. 92 (3) (1988) 714-720.
[23] H.-Q Yin, X.-B yin, Metal-Organic Frameworks with Multiple Luminescence Emissions: Designs and Applications, Acc. Chem. Res. 53 (2) (2020) 485-495.
[24] K. Koren, R.I. Dmitriev, S.M. Borisov, D.B. Papkovsky, I. Klimant, Complexes of Ir(III)octaethylporphyrin with peptides as probes for sensing cellular 0_2, ChemBioChem 13 (8) (2012) 1184-1190.
[25] H. Xiang, J. Cheng, X. Ma, X. Zhou, J.J. Chruma, Near-infrared phosphorescence: materials and applications, Chem. Soc. Rev. 42 (14) (2013) 6128-6185.
[26] K. Kadish, K. Smith, R. Guilard, The Porphyrin Handbook: Phthalocyanines: Spectroscopic and Electrochemical Characterization, 1 ed.16, Academic Press, 2012 1-288.
[27] M. Gouterman, Optical spectra and electronic structure of porphyrins and related rings, in: D. Dolphin (Ed.), The Porphyrins, Academic Press, New York 1978, pp. 1-165.
[28] R. Wiglusz, J. Legendziewicz, A. Graczyk, S. Radzki, P. Gawryszewska, J. Sokolnicki, Spectroscopic properties of porphyrins and effect of lanthanide ions on their luminescence efficiency, J. Alloys Compd. 380 (1) (2004) 396-404.
[29] D. Marsh, L. Mink, Microscale synthesis and electronic absorption spectroscopy of tetraphenylporphyrin H_2 (TPP) and metalloporphyrins ZnII (TPP) and NIII (TPP), J. Chem. Educ. 73 (12) (1996) 1188.
[30] S. Nasri, I. Zahou, I. Turowska-Tyrk, T. Roisnel, F. Loiseau, E. Saint-Amant, H. Nasri, Synthesis, electronic spectroscopy, cyclic voltammetry, photophysics, electrical properties and X-ray molecular structures of meso-{Tetrakis[4-(benzoyloxy)phenyl]porphyrinato}zinc(II) complexes with Aza ligands, Eur. J. Inorg. Chem. 2016 (31) (2016) 5004-5019.
[31] L. Qin, X. Guan, C. Yang, J.-S. Huang, C.-M. Che, Near-infrared phosphorescent supramolecular alkyl/aryl-iridium porphyrin assemblies by axial coordination, Chem. Eur. J. 24 (54) (2018) 14400-14408.
[32] M.J. Kamlet, J.L. Abboud, R.W. Taft, The solvatochromic comparison method. 6. The . pi.* scale of solvent polarities, J. Am. Chem. Soc. 99 (18) (1977) 6027-6038.